

# Free Material Optimization for Laminated Plates and Shells

Alemseged Gebrehiwot Weldeyesus\* and Mathias Stolpe†

## Abstract

Free Material Optimization (FMO) is a powerful approach for conceptual optimal design of composite structures. The design variable in FMO is the entire elastic material tensor which is allowed to vary almost freely over the design domain. The imposed requirements on the tensor are that it is symmetric and positive semidefinite. Most of today's studies on FMO focus on models for two- and three-dimensional structures. The objective of this article is to extend existing FMO models and methods to laminated plate and shell structures, which are used in many engineering applications. In FMO, the resulting optimization problem is generally a non convex semidefinite program with many small matrix inequalities which requires special-purpose optimization methods. The FMO problems are efficiently solved by a primal-dual interior point method developed and implemented by the authors. The quality of the proposed FMO models and the method are supported by several large-scale numerical experiments.

**Mathematics Subject Classification 2010:** 90C22, 90C90, 74P05, 74P15

**Keywords:** Structural optimization, free material optimization, nonlinear semidefinite optimization, laminated shells

---

The research was partially funded by the Danish Council for Strategic Research through the *Danish Center for Composite Structures and Materials* (DCCSM) and the Danish Council for Independent Research — Technology and Production Sciences through the research project *Optimal Design of Composite Structures under Manufacturing Constraints*.

\*DTU Wind Energy, Technical University of Denmark, Frederiksborgvej 399, 4000 Roskilde, Denmark. E-mail: alwel@dtu.dk

†DTU Wind Energy, Technical University of Denmark, Frederiksborgvej 399, 4000 Roskilde, Denmark. E-mail: matst@dtu.dk

# 1 Introduction

In Free Material Optimization (FMO) the design parametrization allows complete control over the entire material tensor. It is allowed vary freely at each point of the design domain with the only requirement that it has to satisfy mild necessary conditions for physical attainability. Therefore, in optimal structures obtained by FMO both the distribution of the amount of material and the optimal local material properties are determined.

The basic concept of FMO was introduced in the early 1990s in [3], [4], and [22]. Since then, several studies led to the development of models, theories, and numerical methods for FMO problems. In the recently proposed FMO problems several types of constraints have been introduced. For example in [15], [14], and [10] problems with constraints on local stresses and displacements and in [26] problems with constraints on fundamental eigenfrequencies are presented and solved. Some of the studies not only emphasize on extending the formulations to multidisciplinary problems but also on development of new optimization methods. The methods include a method based on penalty/barrier multipliers (PBM) in [33] and a method based an augmented Lagrangian function in [13] and [25]. Recently a method based on a sequential convex programming concept [28, 27] and a method based on interior point methods [29] were proposed for FMO. Moreover, detailed theory covering choice of problem formulations and the existence of solutions can be found in [30].

Most of today's FMO studies focus on two- and three-dimensional design domains. In this article we focus on laminated plates and shells which nowadays are used in many engineering applications. There are several approaches to material optimization of such structures. One of them is Discrete Material Optimization (DMO) which was introduced in [23], [24], and [17]. DMO determines the best discrete material selection, stacking sequence, and thickness distribution. An FMO model for Mindlin plate design is introduced in [3]. Later in [9] FMO formulations, analogous to the recent FMO formulations for two- and three-dimensional structures, are proposed for single layer plates and shells. As far as to our knowledge, no FMO models have been proposed for general laminated shell structures. Therefore, we propose new FMO models for laminated plates and shells by extending the formulations in [9].

The requirement of physical attainability of the elastic stiffness tensor leads to a mathematical interpretation that the stiffness tensor must be symmetric positive semidefinite. For this reason, FMO problems result in an optimization problem that belongs to the class of nonlinear semidefinite programming (SDP). We generalize the primal-dual interior point method proposed by the authors in [29] which is especially developed for FMO problems. The method and its implementation exploit the property that FMO problems have many matrix in-

equalities with each inequality involving a small size matrix to efficiently solve large-scale problems. It obtains high quality solutions to large-scale FMO problems within a modest number of iterations.

This article has six sections. In section 2 the shell geometry and kinematics are first described. Then the existing FMO problem formulations for plates and shells are extended to laminated structures. In section 3 the primal-dual interior point method, initially proposed in [29] for two- and some three-dimensional FMO problems, is outlined. Then follows section 4 discussing the implementation of the method and the algorithmic parameters. The numerical experiments, results and discussions are presented in section 5. The conclusions and future research work are in section 6.

## 2 FMO problem formulations

In this section we first describe the geometry of a shell and then specialize solid kinematics to shell kinematics. We follow the approach in [7] and all details can be found therein. At the end of the section, we propose two FMO problem formulations for laminated plates and shells.

### 2.1 Shell kinematics

We refer a shell to a three dimensional structure that has curved inner and outer surfaces with a thickness in the middle of small size compared to other dimensions. Geometrically, a shell is characterized by its midsurface, say  $\mathcal{S} = \phi(\bar{\omega})$ , where  $\phi$  is a smooth injective mapping called a chart from  $\bar{\omega}$ , the closure of the bounded open  $\omega \subset \mathbb{R}^2$ , into  $\mathbb{R}^3$ . The physical three dimensional space occupied by the shell is defined by the chart  $\Phi$  given by

$$\Phi(\xi^1, \xi^2, \xi^3) = \phi(\xi^1, \xi^2) + \xi^3 a_3(\xi^1, \xi^2), \quad (\xi^1, \xi^2, \xi^3) \in \Omega \quad (1)$$

where  $\Omega$  is the 3D reference domain defined by

$$\Omega = \left\{ (\xi^1, \xi^2, \xi^3) \in \mathbb{R}^3 \mid (\xi^1, \xi^2) \in \omega, |\xi^3| < \frac{t(\xi^1, \xi^2)}{2} \right\} \quad (2)$$

with  $t(\xi^1, \xi^2)$  the thickness of the shell at the point  $(\xi^1, \xi^2)$ .

Throughout this section Greek indices and exponents take values in the set  $\{1, 2\}$  while Latin indices and exponents are in the set  $\{1, 2, 3\}$  with the assumption of Einstein summation convention. The local covariant basis vectors that form a basis to the plane tangent to the midsurface are  $a_\alpha = \partial_\alpha \phi$ , and the unit normal basis vector is  $a_3 = (a_1 \times a_2) / \|a_1 \times a_2\|$ . The contravariant local basis vectors  $a^i$  are defined such that they satisfy the relation  $a_i \cdot a^j = \delta_i^j$  where  $\delta_i^j$  is

the Kronecker symbol. The first fundamental form is given by  $a_{\alpha\beta} = a_\alpha \cdot a_\beta$  in covariant form and  $a^{\alpha\beta} = a^\alpha \cdot a^\beta$  in contravariant form. Note that the infinitesimal areas  $dS$  and  $d\xi^1 d\xi^2$  are related as  $dS = \sqrt{a} d\xi^1 d\xi^2$ , where  $a = a_{11}a_{22} - (a_{12})^2$ . The second fundamental form of the surface is defined by  $b_{\alpha\beta} = -a_\alpha \cdot \frac{\partial a_3}{\partial \xi^\beta}$  (and  $b_\beta^\alpha = -a^\alpha \cdot \frac{\partial a_3}{\partial \xi^\beta}$ ). The third fundamental form is given by  $c_{\alpha\beta} = b_\alpha^\lambda b_{\lambda\beta}$ . The surface Christoffel symbols are  $\Gamma_{\beta\alpha}^\lambda = a^\lambda \cdot \frac{\partial a_\beta}{\partial \xi^\alpha}$ . The surface covariant derivative of a vector  $u_\beta$  is defined by  $u_{\beta|\alpha} = \frac{\partial u_\beta}{\partial \xi^\alpha} - \Gamma_{\beta\alpha}^\lambda u_\lambda$ .

Next, we describe the displacement field of the shell through its thickness. This is done by introducing a material line in the direction of  $a_3$ , orthogonal to the midsurface. These material lines are assumed to remain straight and do not experience any elongation in the deformed configuration. Then the displacements of the points located in the material line are

$$U(\xi^1, \xi^2, \xi^3) = u(\xi_1, \xi_2) + \xi^3 \theta_\lambda(\xi_1, \xi_2) a^\lambda(\xi_1, \xi_2) \quad (3)$$

where  $u(\xi_1, \xi_2)$  is the translational displacement of the midsurface. The rotations  $\theta_1$  and  $\theta_2$  of the material line contribute to the displacement  $\xi^3 \theta_\lambda(\xi_1, \xi_2) a^\lambda(\xi_1, \xi_2)$ . For details we again refer the reader to [7]. The above assumption is known as *Reissner-Mindlin kinematical assumption*.

We present the shell model by specializing solid kinematics to shell kinematics as described in [7]. The linear Hooke's law for solid structures reads as

$$\sigma^{ij}(x) = E^{ijkl}(x) e_{kl}(x) \quad (4)$$

where  $E$ ,  $\sigma$  and  $e$  are stiffness, stress and strain tensors, respectively. Referring to the structure of a (single layer) shell that the thickness is small compared to the other dimensions, the material properties are assumed to remain unchanged in the direction normal to the midsurface. Therefore, we assume the midsurface as the surface of symmetry making the shell monoclinic. This leads to some decoupling, see [21], and to the following assumptions on the stiffness tensor for solid structures.

$$\begin{aligned} E^{\alpha\beta\gamma 3} (= E^{\alpha\beta 3\gamma} = E^{\alpha 3\beta\gamma} = E^{3\alpha\beta\gamma}) &= 0, \text{ and} \\ E^{\alpha 333} (= E^{3\alpha 33} = E^{33\alpha 3} = E^{333\alpha}) &= 0. \end{aligned} \quad (5)$$

Using (5) and under the additional assumption that  $\sigma^{33} = 0$  the constitutive equations (4) are modified to

$$\sigma^{\alpha\beta} = C^{\alpha\beta\lambda\mu} e_{\lambda\mu} \text{ and } \sigma^{\alpha 3} = \frac{1}{2} D^{\alpha\lambda} e_{\lambda 3} \quad (6)$$

where

$$C^{\alpha\beta\lambda\mu} = E^{\alpha\beta\lambda\mu} - \frac{E^{\alpha\beta 33} E^{\lambda\mu 33}}{E^{3333}} \text{ and } D^{\alpha\lambda} = 4E^{\alpha 3\lambda 3}. \quad (7)$$

Let  $F$  be an external 3D loading that is applied to the shell structure. The basic shell model is then governed by the variational formulation

$$\begin{aligned} \int_{\Omega} (C^{\alpha\beta\lambda\mu} e_{\alpha\beta}(U) e_{\lambda\mu}(V) + D^{\alpha\lambda} e_{\alpha 3}(U) e_{\lambda 3}(V)) dV \\ = \int_{\Omega} F \cdot V dV \end{aligned} \quad (8)$$

where the unknown  $U$  is of the form (3) satisfying boundary conditions, and  $V$  is a test function fulfilling similar kinematic assumptions and the proper boundary conditions. The displacements in (3) lead to the following expression of the strains in (8),

$$e_{\alpha\beta} = \gamma_{\alpha\beta} + \xi^3 \chi_{\alpha\beta}, \text{ and } e_{\alpha 3} = \zeta_{\alpha}. \quad (9)$$

where  $\gamma_{\alpha\beta}$ ,  $\chi_{\alpha\beta}$  and  $\zeta_{\alpha}$  are the membrane, bending and shear strains of the midsurface that are given by,

$$\gamma_{\alpha\beta}(u) = \frac{1}{2}(u_{\alpha|\beta} + u_{\beta|\alpha}) - b_{\alpha\beta} u_3 \quad (10a)$$

$$\chi_{\alpha\beta}(u, \theta) = \frac{1}{2}(\theta_{\alpha|\beta} + \theta_{\beta|\alpha} - b_{\beta}^{\lambda} u_{\lambda|\alpha} - b_{\alpha}^{\lambda} u_{\lambda|\beta}) - c_{\alpha\beta} u_3 \quad (10b)$$

$$\zeta_{\alpha}(u, \theta) = \frac{1}{2}(\theta_{\alpha} + u_{3,\alpha} + b_{\alpha}^{\lambda} u_{\lambda}). \quad (10c)$$

Next, we write the variational formulation (8) to the lowest order terms for laminated shells of  $N$  layers. We follow [5] to consider the function space  $\mathcal{V}$  defined by

$$\mathcal{V} = \{(u, \theta) \in [H^1(\omega; \mathbb{R}^3)]^2 | \theta \cdot a_3 = 0 \text{ in } \omega, u = \theta = 0 \text{ on } \partial\omega_0\} \quad (11)$$

where  $\partial\omega_0$  is the fixed part of the boundary  $\partial\omega$  of  $\omega$ . The space  $H^1(\omega; \mathbb{R}^3)$  is the standard Sobolev space. We additionally make the assumption that the stiffness tensors are allowed to vary freely across the laminate thickness from layer to layer but not in a layer, that is, they depend of course on  $(\xi_1, \xi_2) \in \omega$ . The loads are assumed not to vary through the thickness. Under this assumption and substituting the strains in the variational formulation (8) by the strains in (9) we obtain the following variational formulation for the laminated shells. Find  $(u, \theta) \in \mathcal{V}$  such that

$$\begin{aligned} \sum_{l=1}^N \int_{\omega} C_l^{\alpha\beta\lambda\mu} \left( t_l \gamma_{\alpha\beta}(u) \gamma_{\lambda\mu}(v) + \tilde{t}_l (\gamma_{\alpha\beta}(u) \chi_{\lambda\mu}(v, \eta) + \right. \\ \left. \gamma_{\lambda\mu}(v) \chi_{\alpha\beta}(u, \theta)) + \tilde{\tilde{t}}_l \chi_{\alpha\beta}(u, \theta) \chi_{\lambda\mu}(v, \eta) \right) dS \\ + \kappa \sum_{l=1}^N \int_{\omega} t_l D_l^{\alpha\lambda} \zeta_{\alpha}(u, \theta) \zeta_{\lambda}(v, \eta) dS = \int_{\omega} tF \cdot v dS \end{aligned} \quad (12)$$

for all  $(v, \eta) \in \mathcal{V}$ , where

$$\begin{aligned} t_l &= t_{l,top} - t_{l,low}, \quad \tilde{t}_l = \frac{1}{2}((t_{l,top})^2 - (t_{l,low})^2), \\ \tilde{\tilde{t}}_l &= \frac{1}{3}((t_{l,top})^3 - (t_{l,low})^3). \end{aligned} \quad (13)$$

The terms  $t_{l,top}$  and  $t_{l,low}$  denote the upper and lower transverse coordinate of the  $l$ th layer at the point  $(\xi^1, \xi^2)$  respectively. The coefficient  $\kappa < 1$  multiplying the shear term is the shear correction factor introduced to consider the shell model which is used in application. The subscript  $l$  in the stiffness tensors  $C_l$  and  $D_l$  implies that stiffnesses belong to the  $l$ th layer. Existence of a unique solution to the variational problem (12) is also shown under natural assumptions for shells in [5].

## 2.2 FMO problem formulations for layered plates and shells

In FMO the design variable is the elastic stiffness tensor, i.e., the tensors  $C$  and  $D$  for the case of laminated plates and shells. They are allowed vary freely at each point of the design domain but required to be physically attainable. Mathematically, they must be symmetric and positive semidefinite, i.e.,  $C = C^T$ ,  $D = D^T$ ,  $C \succeq 0$ , and  $D \succeq 0$ , where  $A \succeq B$  ( $A \succ B$ ) means  $A - B$  is positive semidefinite (positive definite). However, the measure of stiffness is not straight forward. We follow the stiffness measure used in most studies which is the trace of the stiffness tensors. Motivated by [9] and FMO models for solid structures we define the set of admissible materials  $\mathcal{C}$  as

$$\mathcal{C} = \{(C, D) \in [L^\infty(\Omega)]^{3 \times 3} \times [L^\infty(\Omega)]^{2 \times 2} \mid C = C^T \succeq 0, D = D^T \succeq 0\}. \quad (14)$$

The choice of the space of essentially bounded functions  $L^\infty(\omega)$  to define the set of admissible material in (14) is standard in FMO to include the possibilities of material\no material in the optimal designs, see e.g. [2]. The requirement of the factor  $\frac{1}{2}$  can be seen from the relation in (6). The traces are multiplied by the thickness  $t_l$  to conform the surface measure of the shell with the volume measure in three dimensional structures. The trace of the stiffness is locally bounded from above by  $\bar{\rho}$  to avoid arbitrarily stiff material. We also introduce lower trace bounds to make restriction on softness. The bounds on the traces satisfy  $0 \leq \underline{\rho} < \bar{\rho} < \infty$ . The amount of resource material to distribute in the structure is also limited by

$$\sum_{l=1}^N \int_{\omega} t_l \left( \text{Tr}(C_l(x)) + \frac{1}{2} \text{Tr}(D_l(x)) \right) dS \leq \vartheta. \quad (15)$$

with the volume bound  $V$  satisfying  $N|\omega|\underline{\rho} < \vartheta < N|\omega|\bar{\rho}$ , where  $|\omega|$  is the area of  $\omega$ .

Given external loads  $F_\ell, \ell \in L = \{1, \dots, n_L\}$ , we formulate the primal minimum compliance FMO problem as

$$\begin{aligned}
& \underset{(u, \theta)_\ell \in \mathcal{V}, (C, D) \in \mathcal{C}}{\text{minimize}} && \sum_{\ell \in L} w_\ell \int_{\omega} t F_\ell \cdot u_\ell dS \\
& \text{subject to} && (u, \theta)_\ell \text{ satisfying (12) with } F = F_\ell, \forall \ell \in L, \\
& && \underline{\rho} \leq t_l \left( \text{Tr}(C_l(x)) + \frac{1}{2} \text{Tr}(D_l(x)) \right) \leq \bar{\rho}, \forall \ell \in L, \\
& && \sum_{l=1}^N \int_{\omega} t_l \left( \text{Tr}(C_l(x)) + \frac{1}{2} \text{Tr}(D_l(x)) \right) dS \leq \vartheta,
\end{aligned} \tag{16}$$

where  $w_\ell$  are given weights satisfying  $\sum_{\ell} w_\ell = 1$ , and  $w_\ell > 0$  for each  $\ell \in L$ . Alternatively, we formulate the minimum weight FMO problem as

$$\begin{aligned}
& \underset{(u, \theta)_\ell \in \mathcal{V}, (C, D) \in \mathcal{C}}{\text{minimize}} && \sum_{l=1}^N \int_{\omega} t_l \left( \text{Tr}(C_l(x)) + \frac{1}{2} \text{Tr}(D_l(x)) \right) dS \\
& \text{subject to} && (u, \theta)_\ell \text{ satisfying (12) with } F = F_\ell, \forall \ell \in L, \\
& && \underline{\rho} \leq t_l \left( \text{Tr}(C_l(x)) + \frac{1}{2} \text{Tr}(D_l(x)) \right) \leq \bar{\rho}, \forall \ell \in L, \\
& && \sum_{\ell \in L} w_\ell \int_{\omega} t F_\ell \cdot u_\ell dS \leq \mathcal{Y}.
\end{aligned} \tag{17}$$

Note that we do not claim that (16) and (17) are equivalent. The two problems are included since the method and the implementation can solve both. Existence of an optimal solution to FMO problems for *single* layer laminate is shown in [9] under natural assumptions. The problems (16) and (17) have similar mathematical structure to the problem formulation proposed in [9]. Due to the lack of sufficient theoretical results existence of an optimal solution it is *assumed* for now for the problems (16) and (17). The theoretical assumption of existence of solutions should be further investigated and clarified.

### 2.3 Discretization of the FMO problem formulations

We follow the discretization scheme used in [9] and [7]. The reference midsurface  $\omega$  is partitioned in to  $m$  uniform quadrilateral finite elements  $\omega_i$  for  $i = 1, \dots, m$ . We approximate the displacement by a continuous bilinear function. The elastic stiffness tensors  $C(x)$  and  $D(x)$  are approximated by functions that are constant

on each element in each layer. We denote by  $C_{il}$  and  $D_{il}$  the constant approximation of the stiffness tensors  $C$  and  $D$  on the  $i$ th element and  $l$ th layer respectively constituting the vectors of block matrices

$$C = (C_{11}, \dots, C_{1N}, \dots, C_{m1}, \dots, C_{mN})^T$$

and

$$D = (D_{11}, \dots, D_{1N}, \dots, D_{m1}, \dots, D_{mN})^T.$$

Given external static nodal load vectors  $f_\ell^h \in \mathbb{R}^{n_f}$ ,  $\ell \in L$ , where  $n_f$  is number of finite element degrees of freedom, the finite dimensional equilibrium equation of (12) is

$$K(C, D)(u^h, \theta^h)_\ell = f_\ell^h, \ell \in L \quad (18)$$

where  $(u^h, \theta^h)_\ell$  is associated displacement and  $K(C, D)$  is the stiffness matrix given by

$$K(C, D) = \sum_{i=1}^m (K_i^\gamma(C) + K_i^{\gamma\chi}(C) + (K_i^{\gamma\chi}(C))^T + K_i^\chi(C) + K_i^\zeta(D)). \quad (19)$$

In (19), the element stiffness matrices are given by

$$K_i^\gamma(C) = \sum_{l, (j,k) \in n_i} \int_{\omega_i} t_{il} (B_{jl}^\gamma)^T C_{il} B_{kl}^\gamma dS \quad (20a)$$

$$K_i^{\gamma\chi}(C) = \sum_{l, (j,k) \in n_i} \int_{\omega_i} \tilde{t}_{il} (B_{jl}^\gamma)^T C_{il} B_{kl}^\chi dS \quad (20b)$$

$$K_i^\chi(C) = \sum_{l, (j,k) \in n_i} \int_{\omega_i} \tilde{\tilde{t}}_{il} (B_{jl}^\chi)^T C_{il} B_{kl}^\chi dS \quad (20c)$$

$$K_i^\zeta(D) = \kappa \sum_{l, (j,k) \in n_i} \int_{\omega_i} t_{il} (B_{jl}^\zeta)^T D_{il} B_{kl}^\zeta dS, \quad (20d)$$

where  $n_i$  is the index set of nodes associated with the element  $\omega_i$ , and the matrices  $B_{il}^\gamma$ ,  $B_{il}^\chi$  and  $B_{il}^\zeta$  are the (scaled) strain-displacement matrices for membrane strains, for bending strains, and for shear strains, respectively. These are constructed from the derivatives of the shape functions. The factors  $t_{il}$ ,  $\tilde{t}_{il}$  and  $\tilde{\tilde{t}}_{il}$  are computed as in (13) and evaluated at the center of the element  $\omega_i$ .

The discrete primal minimum compliance FMO formulation approximating (16) is

$$\begin{aligned}
& \underset{(u^h, \theta^h)_\ell \in \mathbb{R}^{nf}, (C, D) \in \tilde{\mathcal{C}}}{\text{minimize}} && \sum_{\ell \in L} w_\ell (f_\ell^h)^T (u^h, \theta^h)_\ell \\
& \text{subject to} && K(C, D)(u^h, \theta^h)_\ell = f_\ell^h, \ell \in L, \\
& && \rho \leq t_{il} \left( \text{Tr}(C_{il}) + \frac{1}{2} \text{Tr}(D_{il}) \right) \leq \bar{\rho}, i = 1, \dots, m, \\
& && \sum_{i=1}^m \sum_{l=1}^N t_{il} \left( \text{Tr}(C_{il}) + \frac{1}{2} \text{Tr}(D_{il}) \right) \leq \bar{\vartheta},
\end{aligned} \tag{21}$$

where  $\tilde{\mathcal{C}}$  denotes the set of admissible materials

$$\tilde{\mathcal{C}} = \{ (C, D) \in (\mathbb{R}^{3mN \times 3}) \times (\mathbb{R}^{2mN \times 2}) \mid C_{il} = C_{il}^T \succeq 0, D_{il} = D_{il}^T \succeq 0 \}. \tag{22}$$

The discrete primal minimum weight FMO formulation approximating (17) is

$$\begin{aligned}
& \underset{(u^h, \theta^h)_\ell \in \mathbb{R}^{nf}, (C, D) \in \tilde{\mathcal{C}}}{\text{minimize}} && \sum_{i=1}^m \sum_{l=1}^N t_{il} \left( \text{Tr}(C_{il}) + \frac{1}{2} \text{Tr}(D_{il}) \right) \\
& \text{subject to} && K(C, D)(u^h, \theta^h)_\ell = f_\ell, \ell \in L, \\
& && \rho \leq t_{il} \left( \text{Tr}(C_{il}) + \frac{1}{2} \text{Tr}(D_{il}) \right) \leq \bar{\rho}, i = 1, \dots, m, \\
& && \sum_{\ell \in L} w_\ell (f_\ell^h)^T (u^h, \theta^h)_\ell \leq \bar{\gamma}.
\end{aligned} \tag{23}$$

The problems (21) and (23) are Simultaneous ANalysis and Design (SAND) formulations and belong to the class of non convex SDPs with many linear matrix inequalities. Assuming strict positive definiteness of the stiffness tensors  $C$  and  $D$ , the stiffness matrix  $K(C, D)$  can be assumed to be non singular. Therefore, one can solve for the displacement in the elastic equilibrium equation (18) to eliminate it from the SAND formulations and obtain equivalent nested formulations. However, in [29] it is reported that there is no noticeable difference in the number of iterations the method requires in solving the SAND formulations or the equivalent nested formulations. Moreover, the elastic equilibrium equation needs to be solved at each iteration in the interior point method for the nested formulation. This is found to be an expensive task for large-scale problems. Furthermore, for all problem instances in [29] the non convex SAND formulations give the same optimal designs as the corresponding convex nested formulations. Therefore, we only consider the SAND formulations (21) and (23).

### 3 Outline of the primal-dual interior point method

For completeness and ease of readability we present the general outline of the primal-dual interior method developed in [29]. This entire section is almost identical to Section 3 of [29]. We describe the method for general nonlinear SDP suitable for representing FMO problems in the form

$$\begin{aligned} & \underset{X \in \mathbb{S}, u \in \mathbb{R}^n}{\text{minimize}} && f(X, u) \\ & \text{subject to} && g_j(X, u) \leq 0, \quad j = 1, \dots, k, \\ & && X_i \succeq 0, \quad i = 1, \dots, m, \end{aligned} \quad (24)$$

with

$$\mathbb{S} = \mathbb{S}^{d_1} \times \mathbb{S}^{d_2} \times \dots \times \mathbb{S}^{d_m} \text{ and } (d_1, d_2, \dots, d_m) \in \mathbb{N}^m,$$

and  $\mathbb{S}^d$ -space of symmetric  $d \times d$  matrices. The functions  $f, g_j : \mathbb{S} \times \mathbb{R}^n \rightarrow \mathbb{R}$ , for  $j = 1, \dots, k$  are assumed to be sufficiently smooth. We then formulate the associated barrier problem

$$\begin{aligned} & \underset{X \in \mathbb{S}_+, u \in \mathbb{R}^n, s \in \mathbb{R}_+^k}{\text{minimize}} && f(X, u) - \mu \sum_{i=1}^m \ln(\det(X_i)) - \mu \sum_{j=1}^k \ln(s_j) \\ & \text{subject to} && g_j(X, u) + s_j = 0, \quad j = 1, \dots, k. \end{aligned} \quad (25)$$

where  $s \in \mathbb{R}_+^k$  are slack variables and  $\mu > 0$  is barrier parameter. We solve this barrier problem for a monotonically decreasing sequence of barrier parameter  $\mu_k$  that approaches zero. In that case the barrier problem also approaches the original problem (24). The Lagrangian to problem (25) is

$$\begin{aligned} \mathcal{L}_\mu(X, u, s, \lambda) = & f(X, u) - \mu \sum_{i=1}^m \ln(\det(X_i)) - \mu \sum_{j=1}^k \ln(s_j) \\ & + \lambda^T (g(X, u) + s), \end{aligned} \quad (26)$$

where  $\lambda \in \mathbb{R}_+^k$  is Lagrangian multiplier. Problem (25) has the KKT conditions

$$\begin{aligned} \nabla_X \mathcal{L}_\mu(X, u, s, \lambda) = \nabla_X f(X, u) - \mu X^{-1} + \nabla_X (g(X, u))^T \lambda \\ = 0 \end{aligned} \quad (27a)$$

$$\nabla_u \mathcal{L}_\mu(X, u, s, \lambda) = \nabla_u f(X, u) + \nabla_u g(X, u)^T \lambda = 0 \quad (27b)$$

$$\nabla_s \mathcal{L}_\mu(X, u, s, \lambda) = -\mu S^{-1} e + \lambda = 0 \quad (27c)$$

$$g(X, u) + s = 0 \quad (27d)$$

$$X \succ 0, s > 0, \lambda > 0 \quad (27e)$$

where  $S = \text{diag}(s)$  and  $e = (1, 1, \dots, 1)^T$  is a vector of all ones of appropriate size. We modify the optimal conditions by making the substitution  $Z := \mu X^{-1}$  in (27a) and including additional equation

$$XZ - \mu I = 0. \quad (28)$$

It is important that the product  $XZ$  in (28) has to be symmetric to get a square system. We use the linear operator  $H_P : \mathbb{R}^{n \times n} \rightarrow \mathbb{S}^n$ , introduced in [32] and defined by

$$H_P(Q) := \frac{1}{2} (PQP^{-1} + (PQP^{-1})^T)$$

where  $P \in \mathbb{R}^{n \times n}$  is some non-singular matrix to achieve the symmetry. The complementarity condition (28) is then replaced by

$$H_P(XZ) - \mu I = 0. \quad (29)$$

The directions obtained by setting the matrices  $P$  are called members of the Monteiro-Zhang (MZ) family [32]. The most commonly used search directions are the AHO direction [1] obtained when  $P = I$ , the HRVW/KSH/M direction [11, 12, 18] when  $P = Z^{1/2}$ , the dual HRVW/KSH/M direction [12, 18] when  $P = X^{-1/2}$ , and the NT direction [19, 20] when  $P = W^{-1/2}$  with  $W = X^{1/2}(X^{1/2}ZX^{1/2})^{-1/2}X^{1/2}$ . In this article the NT direction is used based on the recommendation in [29] for its robustness in solving FMO problems.

We apply Newton's method to solve the KKT system. We further use the operator  $P \odot Q : \mathbb{S}^n \rightarrow \mathbb{S}^n$  defined by

$$(P \odot Q)K := \frac{1}{2}(PKQ^T + QKP^T).$$

to write the Newton system. In FMO the coefficient matrix in the Newton system has block diagonal matrices where each block matrix is small and relatively cheap to invert. Therefore, we only present the reduced saddle point system in  $(\Delta u, \Delta \lambda) \in \mathbb{R}^n \times \mathbb{R}^k$  as

$$\begin{pmatrix} G & A \\ A^T & B \end{pmatrix} \begin{pmatrix} \Delta u \\ \Delta \lambda \end{pmatrix} = \begin{pmatrix} \tilde{r}_d \\ \tilde{r}_p \end{pmatrix} \quad (30)$$

where

$$\begin{aligned} G &= \nabla_{uu}^2 \mathcal{L}_\mu(X, u, s, \lambda) \\ &\quad - \nabla_{Xu}^2 \mathcal{L}_\mu(X, u, s, \lambda) \tilde{H}^{-1} \nabla_{Xu}^2 \mathcal{L}_\mu(X, u, s, \lambda)^T \\ A &= \nabla_u g(X, u)^T - \nabla_{Xu}^2 \mathcal{L}_\mu(X, u, s, \lambda)^T \tilde{H}^{-1} \nabla_X g(X, u)^T \\ B &= -\Lambda^{-1} S - \nabla_X g(X, u) \tilde{H}^{-1} \nabla_X g(X, u)^T. \end{aligned}$$

The right hand sides in (30) are computed as

$$\begin{aligned}\tilde{r}_d &= r_d - \nabla_{Xu}^2 \mathcal{L}_\mu(X, u, s, \lambda) \tilde{H}^{-1}(R_d + \mathcal{F}^{-1} R_C) \\ \tilde{r}_p &= r_p - \Lambda^{-1} r_c - \nabla_X g(X, u) \tilde{H}^{-1}(R_d + \mathcal{F}^{-1} R_C)\end{aligned}$$

with  $(R_d, r_d, r_c, r_p, R_C)^T$  denoting the negative of left hand side of the systems (27) and (29). The other search directions  $(\Delta X, \Delta s, \Delta Z) \in \mathbb{S} \times \mathbb{R}^k \times \mathbb{S}$  are then computed as

$$\begin{aligned}\Delta X &= \tilde{H}^{-1}(R_d + \mathcal{F}^{-1} R_C - \nabla_{Xu}^2 \mathcal{L}_\mu(X, u, s, \lambda)^T \Delta u \\ &\quad - \nabla_X g(X, u)^T \Delta \lambda)\end{aligned}\tag{31a}$$

$$\Delta Z = \mathcal{F}^{-1}(R_C - \mathcal{E} \Delta X)\tag{31b}$$

$$\Delta s = \Lambda^{-1}(r_c - S \Delta \lambda).\tag{31c}$$

For the complete details of the Newton system and the (tensor) products, see Section 3 and Appendix B of [29]. In (31) the block diagonal matrices  $\mathcal{E} = \mathcal{E}(X, Z)$  and  $\mathcal{F} = \mathcal{F}(X, Z)$  are the derivatives of  $H_P(XZ)$  with respect to  $X$  and  $Z$  respectively and are given by

$$\mathcal{E} = P \odot P^{-T} Z \text{ and } \mathcal{F} = P X \odot P^{-1}.\tag{32}$$

Given a current iterate  $(X, u, s, \lambda, Z)$  and a search direction  $(\Delta X, \Delta u, \Delta s, \Delta \lambda, \Delta Z)$  we perform the standard steps in interior point methods to determine the primal step length  $\alpha_p$  and dual step length  $\alpha_d$ . We first determine the maximum possible step to the boundary region

$$\begin{aligned}\bar{\alpha}_p &= \max\{\alpha \in (0, 1] : X + \alpha \Delta X \succeq (1 - \tau)X, \\ &\quad s + \alpha \Delta s \geq (1 - \tau)s\}\end{aligned}\tag{33a}$$

$$\begin{aligned}\bar{\alpha}_d &= \max\{\alpha \in (0, 1] : Z + \alpha \Delta Z \succeq (1 - \tau)Z, \\ &\quad \lambda + \alpha \Delta \lambda \geq (1 - \tau)\lambda\}\end{aligned}\tag{33b}$$

where  $\tau \in (0, 1)$  is the fraction to the boundary parameter. Next follows a backtracking line-search to get sufficient decrease in the merit function  $\phi_\mu$  defined by

$$\begin{aligned}\phi_\mu(X, u, s, \lambda, Z) &:= \|\nabla_X f(X, u) - Z + \nabla_X (g(X, u)^T \lambda)\|_F^2 \\ &\quad + \|(S\Lambda - \mu I)e\|_2^2 + \|g(X, u) + s\|_2^2 \\ &\quad + \|\nabla_u f(X, u) + \nabla_u g(X, u)^T \lambda\|_2^2 \\ &\quad + \|H_P(XZ) - \mu I\|_F^2.\end{aligned}\tag{34}$$

where  $\|\cdot\|_F$  is Frobenius norm. A search direction decreases sufficiently the merit function if

$$\begin{aligned} \phi_\mu(X + \alpha_p \Delta X, u + \alpha_p \Delta u, s + \alpha_p \Delta s, \lambda + \alpha_d \Delta \lambda, Z + \alpha_d \Delta Z) \\ \leq (1 - \tau_0 \eta) \phi_\mu(X, u, s, \lambda, Z) \end{aligned} \quad (35)$$

for a parameter  $\eta \in (0, 1)$  and for a constant  $\tau_0 \in (0, 1)$ . The final step lengths are then

$$\alpha_p \in (0, \bar{\alpha}_p], \text{ and } \alpha_d \in (0, \bar{\alpha}_d].$$

The new iterate  $(X^+, u^+, s^+, \lambda^+, Z^+)$  is

$$(X^+, u^+, s^+) = (X, u, s) + \alpha_p (\Delta X, \Delta u, \Delta s) \quad (36a)$$

$$(\lambda^+, Z^+) = (\lambda, Z) + \alpha_d (\Delta \lambda, \Delta Z). \quad (36b)$$

The algorithm terminates when

$$\begin{aligned} \max \left\{ \max_i \|\nabla_{X_i} f(X, u) - Z_i + \nabla_{X_i} (g(X, u)^T \lambda)\|_F, \right. \\ \left. \|\nabla_u f(X, u) + \nabla_u g(X, u)^T \lambda\|_\infty \right\} \leq \epsilon^o \\ \max \left\{ \max_i \|H_P(X_i Z_i)\|_F, \|S \Lambda e\|_\infty \right\} \leq \epsilon^o \\ \|g(X, u)_+\|_\infty \leq \epsilon^f \end{aligned} \quad (37)$$

where  $g_j(X, u)_+ = \max\{0, g_j(X, u)\}$ , and  $\epsilon^o > 0$  and  $\epsilon^f > 0$  are respectively given optimality and feasibility tolerances of the original problem (24). For the barrier problem (25) we determine the optimality tolerance  $\epsilon_\mu^o$  and feasibility tolerance  $\epsilon_\mu^f$  through

$$\epsilon_\mu^o = \max\{10\mu, \epsilon^o - \mu\}, \quad \text{and} \quad \epsilon_\mu^f = \max\{10\mu, \epsilon^f\}. \quad (38)$$

They thus become  $\mu$  dependent such that the method performs few inner iterations in the first outer iterations. The inner iteration loop stops when

$$\begin{aligned} \max \left\{ \max_i \|\nabla_{X_i} f(X, u) - Z_i + \nabla_{X_i} (g(X, u)^T \lambda)\|_F, \right. \\ \left. \|\nabla_u f(X, u) + \nabla_u g(X, u)^T \lambda\|_\infty \right\} \leq \epsilon_\mu^o \\ \max \left\{ \max_i \|H_P(X_i Z_i) - \mu I\|_F, \|S \Lambda e - \mu e\|_\infty \right\} \leq \epsilon_\mu^o \\ \|g(X, u) + S\|_\infty \leq \epsilon_\mu^f. \end{aligned} \quad (39)$$

For each barrier problem we estimate the barrier parameter  $\mu$  by

$$\mu = \sigma \left( \sum_i \text{Tr}(X_i^T Z_i) / d_i + s^T \lambda \right) / (m + k), \quad \sigma < 1 \quad (40)$$

which is proportional to the gap between the objective functions of the primal and the dual problems.

The overall description of the interior point method is given in Algorithm 1. The algorithm is identical to the algorithm in [29].

---

**Algorithm 1** A primal-dual interior point algorithm for nonlinear SDP problems (from [29]).

---

Choose  $w_p^0 = (X^0, u^0, s^0)$ ,  $w_d^0 = (\lambda, Z)$ , and  $\mu_0$  as in (40).  
Set the outer iteration counter  $k \leftarrow 0$ .  
**while** stopping criteria (37) for problem (24) is not satisfied and  $k < k_{max}$  **do**  
  Set the inner iteration counter  $i \leftarrow 0$   
  **while** stopping criteria (39) for problem (25) is not satisfied and  $i < i_{max}$  **do**  
    Compute the search direction  $\Delta w_p^{k,i}$  and  $\Delta w_d^{k,i}$  by solving system (30) and (31).  
    Compute  $\bar{\alpha}_p$  and  $\bar{\alpha}_d$  as in (33).  
    Set the line search iteration counter  $l \leftarrow 0$ .  
    Set **LineSearch**  $\leftarrow$  **False**  
    **while** **LineSearch** = **False** and  $l < l_{max}$  **do**  
       $\alpha_p \leftarrow \eta^l \bar{\alpha}_p$  and  $\alpha_d \leftarrow \eta^l \bar{\alpha}_d$   
      **if**  $\phi_\mu(w_p^{k,i} + \alpha_p \Delta w_p^{k,i}, w_d^{k,i} + \alpha_d \Delta w_d^{k,i}) \leq (1 - \tau_0 \eta^l) \phi_\mu(w_p^{k,i}, w_d^{k,i})$  **then**  
        Set the new iterate  $(w_p^{k,i+1}, w_d^{k,i+1})$  as in (36).  
        **LineSearch**  $\leftarrow$  **True**  
      **else**  
         $l \leftarrow l + 1$ .  
      **end if**  
    **end while**  
     $i \leftarrow i + 1$ .  
  **end while**  
  Update  $\mu_{k+1}$  as in (40).  
   $k \leftarrow k + 1$ .  
**end while**

---

## 4 Implementation, algorithmic parameters, and problem data

The code implemented and described in [29] to solve FMO problems for two- and three-dimensional FMO problems is generalized and used to solve the FMO problems for laminated plates and shells presented in section 2. The algorithm, the

Table 1: Algorithmic parameters and initial points used in the implementation of the primal-dual interior point method.

Parameters/ initial points	Values
Optimality tolerance $\epsilon^o$	$10^{-6}$
Feasibility tolerance $\epsilon^f$	$10^{-7}$
Minimum barrier parameter value $\mu_{\min}$	$10^{-8}$
Boundary to the fraction parameter $\tau$	0.9
$\eta$ - line-search parameter in (35)	0.5
$\tau_0$ - line-search parameter in (35)	$10^{-5}$
Centrality constant $\sigma$	0.4
Initial stiffness tensors $C_{il}$ and $D_{il}$	$0.1\bar{\rho}I$ for all $i$ and $l$
Initial displacement vectors $u_\ell$	0 for all $\ell$
Initial slack variables	1
Initial Lagrange multipliers for equality constraints	0
Initial Lagrange multipliers for scalar (or matrix) inequality constraints	1 (or $I$ )

parameters and choice of primal and dual initial points are kept unaltered except with minor changes to make the code suitable for the problems in this article. The interior point method and the finite element routines are implemented entirely in MATLAB Version 7.7. All numerical experiments are run on Intel Xeon X5650 six-core CPUs running at 2.66 GHz with 4GB of memory per core (only a single core is used per problem). The standard quadrangular CQUAD4 elements with six degrees of freedom per node are considered with full Gaussian integration layer wise and explicit integration over the thickness. The implementation of the finite element is exactly as described in [9].

The saddle point systems resulting from the application of Newton's method to solve the KKT conditions are solved using the *LDL* factorization routines which are built into MATLAB. We use the NT direction since numerical experiments in [29] show that the NT directions are more robust compared to the other AHO and HRVW/KSV/M directions.

The minimum compliance problems are, for all problem instances, solved with the total weight fraction set to 40% of the maximum possible weight. The algorithmic parameter values and choice of initial points used in the implementation are listed in Table 1. The local bounds on the box constraints are scaled such that  $\bar{\rho}/\rho = 10^5$ .

Table 2: FMO problem instances.

Problems	No. of layers	No. of FEs	No. of linear matrix inequalities	No. of design variables	No. of non-fixed state variables
Michell beam	4	20000	160000	720000	121200
Plate	8	40000	640000	2880000	237606
Spherical cap	8	10000	160000	720000	60006
Cylindrical cap	1	80000	160000	720000	483486
Cylinder	1	40000	80000	360000	240000
Shell beam (two load cases)	1	12800	25600	115200	76320

## 5 Numerical experiments

In this section we report numerical results for six examples. To the best of our knowledge there are no other benchmark FMO problems for laminated plates and shells reported in literature with which we can compare our results. Nevertheless, for some of the examples we refer to results obtained by two-dimensional FMO problems or other structural optimization approaches such as DMO. However, these comparisons are only qualitative.

In all examples the normalized dimension of the spanned domain region is  $1 \times 1$  if it is square and  $1 \times 2$  if it is rectangular except for the shell beam in Example 5.6 where the dimensions are  $1 \times 8$ . The thickness is 0.01 times the length of the shortest dimension of spanned region. If the laminate has multiple layers then the thickness is divided evenly over the layers and numbering is from bottom layer to top layer. The problem instances are presented in Table 2. We refer the optimal density distribution to the trace of the optimal stiffness tensor and its plots scales to the color bar shown in Figure 1. The realization of solutions to FMO problems is in general difficult. There are some tools that have been developed to interpret FMO solutions, see e.g. [6]. Fiber reinforced composite structures could be one choice particularly for the results from this article. In that case the determination of fiber angle is important which is not however a design variable in FMO problems. Nevertheless, we report plots for the in-plane strain field computed via the eigenvectors of the strain tensors for some of the examples.

The computational time and number of iterations required to obtain solutions for the problem instances in Table 2 are reported in Table 3. The numerical figures in these tables show that the FMO problems are large-scale problems. The optimal designs are obtained within 50 and 60 iterations. This is modest for methods for nonlinear SDPs and so the efficiency of the method is implied.



Figure 1: Colorbar for the optimal density distribution.

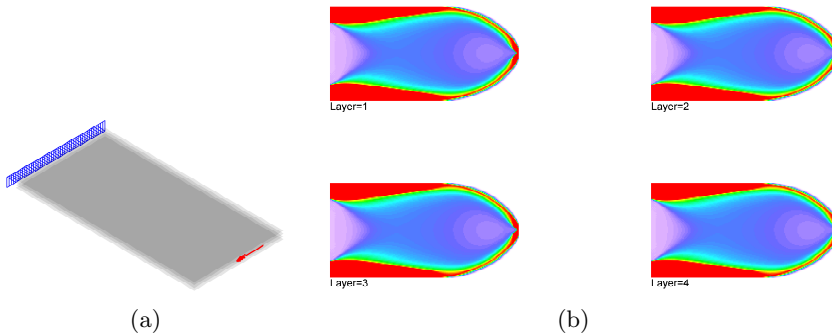


Figure 2: Design domain, boundary conditions, and external load (a), optimal density distribution (b) of the Michell beam consisting of four layers. The density distribution is identical in all layers as expected.

Studying the history of the iteration we also find that the direct solution of the saddle point system dominates the computation time of the method. This is also illustrated in Table 3 where the computational time in solving multiple load FMO problems dramatically increases.

**Example 5.1.** In the first example we consider a laminate of four plate layers clamped at one edge and subject to a pure in-plane load at the opposite edge as shown in Figure 2a. This example is included to show consistency of the models. The model gives results that are similar to solutions to two-dimensional FMO problem in [33] and Variable Thickness Sheet problem in [8]. Figure 2b shows that there is no distinction among the density distribution of the layers. The numerical values of the optimal solution also show that stiffness tensor  $C$  that accounts for membrane deformation dominates the tensor  $D$  (which is zero over the entire design domain). The traverse displacements are also zero. The in-plane strain field for the bottom layer is plotted in Figure 3. The other three layers have identical strain fields.

**Example 5.2.** In this example we consider a clamped laminate of eight plate layers subject to a uniformly distributed load, see Figure 4a. In the optimal

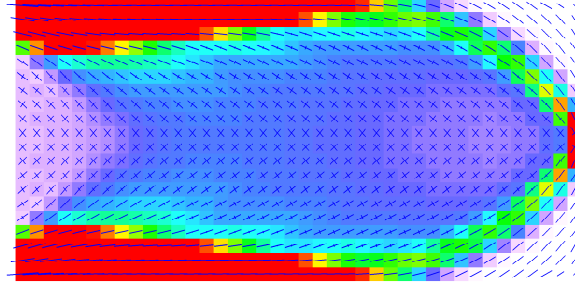


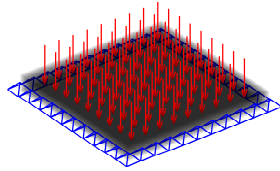
Figure 3: In-plane strain field of layer 1 for the Michell beam problem.

density distribution, shown in Figure 4b, the large interconnected reinforcement in the surface layers splits in to smaller edge and center reinforcements in the next inner layers and then ends up in soft material in the innermost layers. This property resembles the expected sandwich structures. The in-plane strain field of the lower left corners of the bottom four layers is plotted in Figure 5. These strain fields also correspond to that of the top four layers of equidistant from the midsurface. Therefore, the solution implies a symmetric laminate.

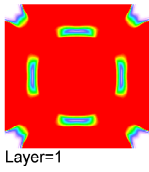
**Example 5.3.** We consider a hinged spherical cap of 8 layers subject to a single transversal load concentrated at the center as shown in the Figure 6a. The geometry of the shell is adapted from [24]. The plot for the optimal distribution of materials is shown Figure 6b. There are wider stiff regions in the surface layers than the inner layers with the center reinforcement appearing in all layers. However, the symmetry behavior of the density distribution with respect to the midsurface does not exist. We can also find the correspondence of the solution to a sandwich structure and the unsymmetrical behavior in a solution to a similar DMO problem in [24].

**Example 5.4.** The design domain is a corner hinged cylindrical cap loaded by a transversal load concentrated at the center as shown in Figure 7a. The plot for the optimal density distribution in Figure 7b shows the cross-like topology extending from the center to the corners which can be found in other structural optimization approaches, see e.g., [16].

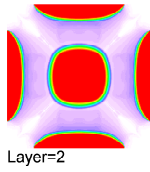
**Example 5.5.** In this example a cylinder is clamped at one end and is subject to a load distributed on a small curve in the opposite end. All the nodal values of



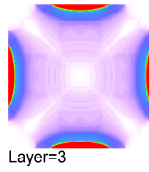
(a)



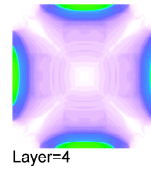
Layer=1



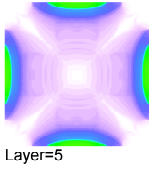
Layer=2



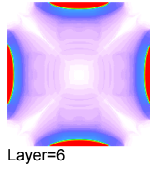
Layer=3



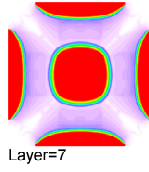
Layer=4



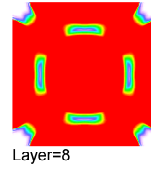
Layer=5



Layer=6



Layer=7



Layer=8

(b)

Figure 4: Design domain, boundary conditions, and external load (a), optimal density distribution (b) of the clamped plate consisting of eight layers.

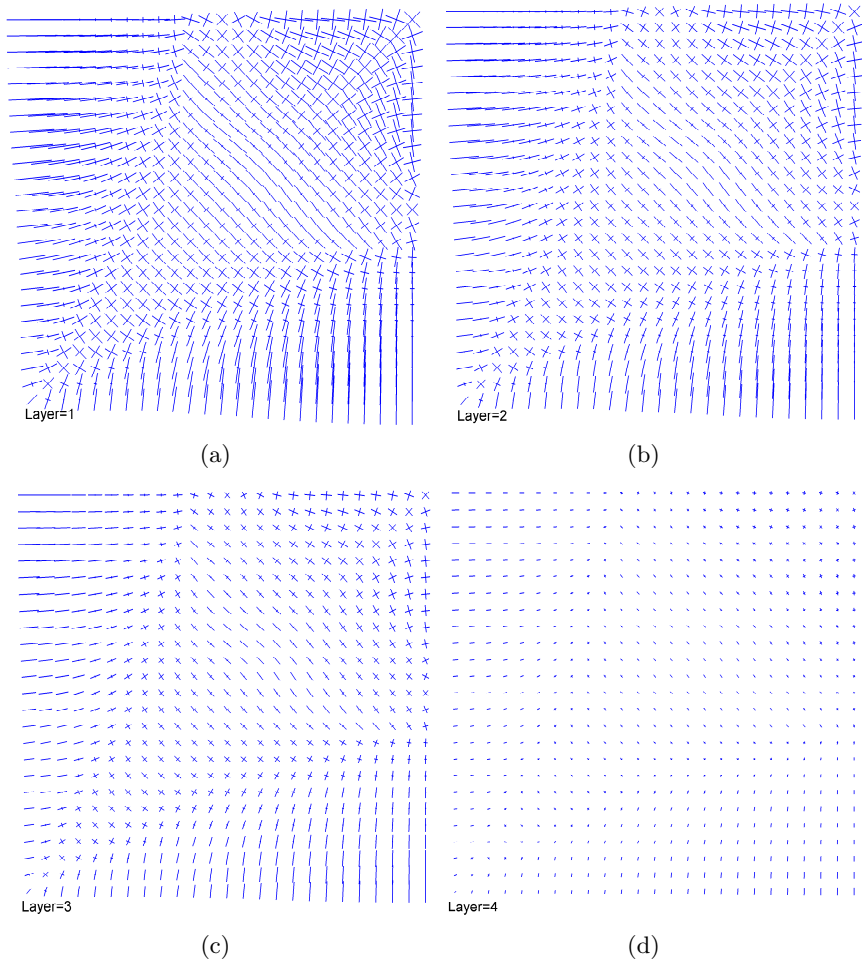
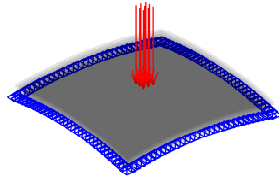
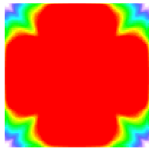


Figure 5: In-plane strain field of the bottom four layers of the lower left quarters for the plate problem.



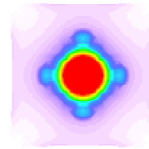
(a)



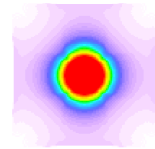
Layer=1



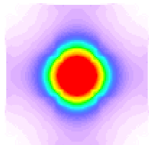
Layer=2



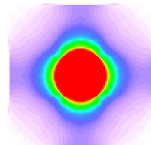
Layer=3



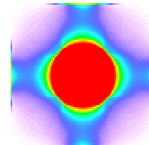
Layer=4



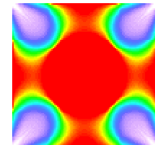
Layer=5



Layer=6



Layer=7



Layer=8

(b)

Figure 6: Design domain, boundary conditions, and external load (a), optimal density distribution (b) of the hinged spherical cap of eight layers.

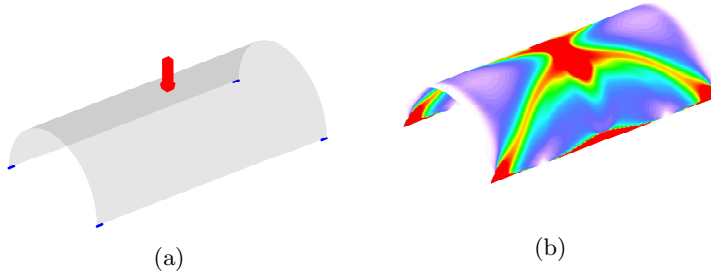


Figure 7: Design domain, boundary conditions, and external load (a), optimal density distribution (b) of the single layered cylindrical cap hinged at the four corners.

the load point in the same direction, see Figure 8a. The usual topology obtained when solving a two-dimensional cantilever beam problem, see e.g., [29], can be seen in Figure 8b spanning from the loading curve to the fixed base on both halves of the cylinder.

**Example 5.6.** We consider a shell beam clamped at both ends subject to two independent loads distributed over lines lying at the middle of opposite lateral surfaces as show in the Figure 9a. In the optimal design Figure 9b the stiff regions around the loading lines are extended and connected to the fixed regions forming a chain of diamond-like topology over the top and bottom surfaces. The response of the diamond like topology shows up in solutions to two-dimensional FMO problem on a rectangular design domain clamped at its two opposite edges and subject to two independent loads at the center of the other tow edges pointing in opposite directions, see [33]. Similar topology of the loaded surfaces can also be found in [31] while solving a single load problem over a three surface shell beam.

## 6 Conclusions

We extended existing FMO models and a primal-dual interior point method for plates and shells to laminated structures for the first time. The consistency of the model is shown first by solving a well-known Michell beam problem under

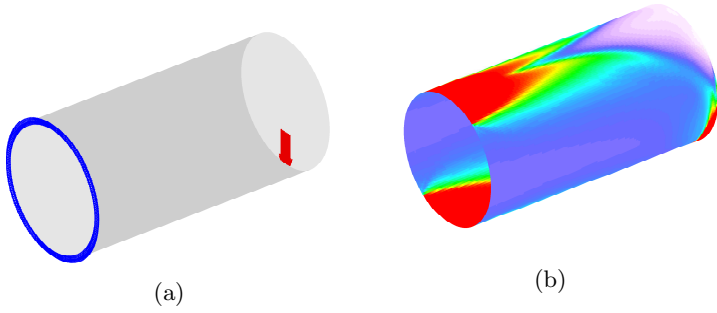


Figure 8: Design domain, boundary conditions, and external load (a), optimal density distribution (b) of the single layered cylinder clamped at one end.

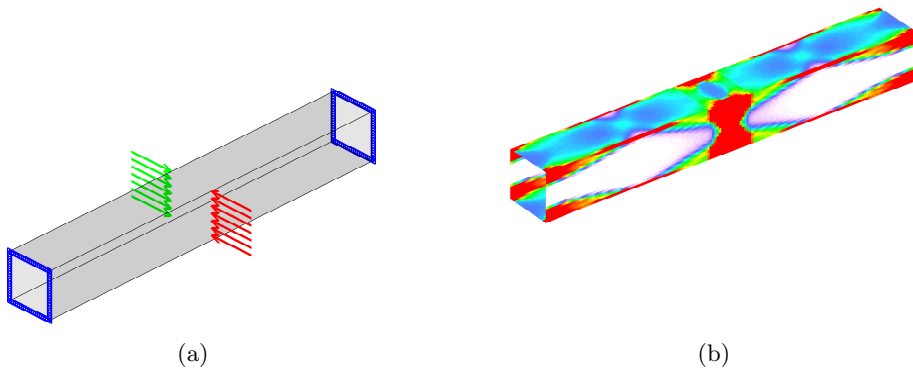


Figure 9: Design domain, boundary condition, and external loads (a), optimal density distribution (b) of the single layered rectangular pipe clamped at both ends.

Table 3: Numerical results for the problem instances in Table 2 and the minimum compliance problem (16).

Problems	No. of iterations	CPU time (hr:min:sec)
Michell beam	52	02:01:27
Plate	60	10:41:45
Spherical cap	54	02:06:44
Cylindrical cap	52	03:26:36
Cylinder	51	01:34:58
Shell beam (two load cases)	50	04:39:50

an in-plane load where the optimal designs of the layers are found to be identical. During transversal loading situations and multilayer laminate the obtained optimal designs correspond to sandwich structures. Similar designs have also been found by other structural optimization approaches such as Discrete Material Optimization and classical topology optimization. The authors are currently working on problem formulations including constraints on local properties such as stresses and strains.

The behaviour of the interior point method and its implementation initially introduced for FMO for two- and three-dimensional problems in [29] and now modified for FMO problems for plates and shells are not altered. In general the method is efficient, requires a modest number of iterations that increase very slowly with problem size, and gives high quality solutions.

## Acknowledgements

We would like to express our sincere gratitude to our colleague José Pedro Blasques for many and fruitful discussions on optimal design of composite structures.

## References

- [1] Alizadeh, F., Haeberly, J.A., Overton, M.L.: Primal-dual interior-point methods for semidefinite programming: convergence rates, stability and numerical results. *SIAM Journal on Optimization* **8**(3), 746–768 (2009)
- [2] Ben-Tal, A., Nemirovski, A.: Robust truss topology design via semidefinite programming. *SIAM Journal on Optimization* **7**(4), 991–1016 (1997)

- [3] Bendsøe, M.P., Díaz, A.R.: Optimization of material properties for Mindlin plate design. *Structural Optimization* **6**, 268–270 (1993)
- [4] Bendsøe, M.P., Guedes, J.M., Haber, R.B., Pedersen, P., Taylor, J.E.: An analytical model to predict optimal material properties in the context of optimal structural design. *Journal of Applied Mechanics* **61**, 930–937 (1994)
- [5] Blouza, A., Dret, H.L.: Nagdhi’s shell model: Existence, uniqueness and continuous dependence on the midsurface. *Journal of elasticity* **64**, 199–216 (2001)
- [6] Bodnár, G., Stadelmeyer, P., Bogomolny, M.: Methods for computer aided interpretation of FMO results. Tech. rep., PLATO-N Public Report PU-R-3-2008 (2008). Available from <http://www.plato-n.org/>
- [7] Chapelle, D., Bathe, K.J.: *The Finite Element Analysis of Shells - Fundamentals*. Springer, Heidelberg (2003)
- [8] Czarnecki, S., Lewiński, T.: On minimum compliance problems of thin elastic plates of varying thickness. *Structural and Multidisciplinary Optimization* **48**(1), 17–31 (2013)
- [9] Gaile, S.: Free material optimization for shells and plates. Ph.D. thesis, Institute of Applied Mathematics II, Friedrich-Alexander University of Erlangen-Nuremberg (2011). Available from <http://www.researchgate.net/>
- [10] Haslinger, J., Kočvara, M., Leugering, G., Stingl, M.: Multidisciplinary free material optimization. *SIAM Journal on Applied Mathematics* **70**(7), 2709–2728 (2010)
- [11] Helmberg, C., Rendl, F., Vanderbei, R.J., Wolkowicz, H.: An interior-point method for semidefinite programming. *SIAM Journal on Optimization* **6**, 342–361 (1996)
- [12] Kojima, M., Shindoh, S., Hara, S.: Interior-point methods for the monotone semidefinite linear complementarity problem in symmetric matrices. *SIAM Journal on Optimization* **7**(1), 86–125 (1997)
- [13] Kočvara, M., Stingl, M.: A code for convex nonlinear and semidefinite programming. *Optimization Methods and Software* **18**(3), 317–333 (2003)
- [14] Kočvara, M., Stingl, M.: Free material optimization for stress constraints. *Structural and Multidisciplinary Optimization* **33**, 323–355 (2007)
- [15] Kočvara, M., Stingl, M., Zowe, J.: Free material optimization: recent progress. *Optimization* **57**(1), 79–100 (2008)

- [16] Lee, S.J., Bae, J.E., Hinton, E.: Shell topology optimization using the layered artificial material model. *International Journal for Numerical Methods in Engineering* **47**, 843–867 (2000)
- [17] Lund, E., Stegmann, J.: On structural optimization of composite shell structures using a discrete constitutive parametrization. *Wind Energy* **8**, 109–124 (2005)
- [18] Monteiro, R.D.C.: Primal-dual path-following algorithms for semidefinite programming. *SIAM Journal on Optimization* **7**(3), 663–678 (1997)
- [19] Nesterov, Y.E., Todd, M.J.: Self-scaled barriers and interior-point methods for convex programming. *Mathematics of Operations Research* **22**(1), 1–42 (1997)
- [20] Nesterov, Y.E., Todd, M.J.: Primal-dual interior-point methods for self-scaled cones. *SIAM Journal on Optimization* **8**(2), 324–364 (1998)
- [21] Reddy, J.: *Mechanics of laminated composite plates and shells: theory and analysis*, 2nd edn. London (2004)
- [22] Ringertz, U.T.: On finding the optimal distribution of material properties. *Structural Optimization* **5**, 265–267 (1993)
- [23] Stegmann, J.: Analysis and optimization of laminated composite shell structures. Ph.D. thesis, Institute of Mechanical Engineering, Aalborg University, Aalborg, Denmark (2004). Available from <http://www.researchgate.net/>
- [24] Stegmann, J., Lund, E.: Discrete material optimization of general composite shell structures. *International Journal for Numerical Methods in Engineering* **62**, 2009–2007 (2005)
- [25] Stingl, M.: On the solution of nonlinear semidefinite programs by augmented lagrangian method. Ph.D. thesis, Institute of Applied Mathematics II, Friedrich-Alexander University of Erlangen-Nuremberg (2006). Available from <http://www2.am.uni-erlangen.de/>
- [26] Stingl, M., Kočvara, M., Leugering, G.: Free material optimization with fundamental eigenfrequency constraints. *SIAM Journal on Optimization* **20**(1), 524–547 (2009)
- [27] Stingl, M., Kočvara, M., Leugering, G.: A new non-linear semidefinite programming algorithm with an application to multidisciplinary free material optimization. *International Series of Numerical Mathematics* **158**, 275–295 (2009)

- [28] Stingl, M., Kočvara, M., Leugering, G.: A sequential convex semidefinite programming algorithm with an application to multiple-load free material optimization. *SIAM Journal on Optimization* **20**(1), 130–155 (2009)
- [29] Weldeyesus, A.G., Stolpe, M.: A primal-dual interior point method for large-scale free material optimization. *Computational Optimization and Applications* (2014). DOI 10.1007/s10589-014-9720-6
- [30] Werner, R.: Free material optimization-mathematical analysis and numerical solution. Ph.D. thesis, Institute of Applied Mathematics II, Friedrich-Alexander University of Erlangen-Nuremberg (2001)
- [31] Yang, B.J., Chen, C.J.: Stress-based topology optimization. *Structural Optimization* **12**, 98–105 (1996)
- [32] Zhang, Y.: On extending some primal-dual interior-point algorithms from linear programming to semidefinite programming. *SIAM Journal on Optimization* **8**(2), 365–386 (1998)
- [33] Zowe, J., Kočvara, M., Bendsøe, M.P.: Free material optimization via mathematical programming. *Mathematical Programming* **79**, 445–466 (1997)